A method for determination of free surface energy and adhesion forces. Highly dispersed oxides, mesoporous and microporous materials

V.V. Turov[1], V.M. Gun'ko[1], R. Leboda[2] and V.V. Brei[1]

[1]Institute of Surface Chemistry, 17 General Naumov Street,
03164 Kiev, Ukraine

[2]Uniwersytet Marii Curie-Skłodowskiej, Wydział Chemii
Pl. M. C. Skłodowskiej 3, 20-031 Lublin, Poland

A method of determination of the Gibbs free surface energy and the radial dependence of adhesion forces of adsorbents in respect to the interfacial water was developed on the basis of measurements of the ^1H NMR signal intensity of unfrozen water at T < 273K. It was considered features of application of this method to highly disperse oxides, modified oxides, microporous and mesoporous adsorbents. The free surface energy values are computed for a variety of oxide and carbon-mineral materials.

1. INTRODUCTION

NMR spectroscopy is widely used to study the structure of solids and a significant portion of the results has been obtained utilizing the solid-state spectroscopy of high resolution with magic-angle spinning and cross-polarization (CP-MAS) or combination of the rotation with the multi-pulse spectroscopy (CRAMS). Exploration of interaction between adsorbed molecules and solid surfaces can be based on the measurements of the temperature dependencies of longitudinal and cross-relaxation of nuclear spins of adsorbates [1]. The mobility of adsorbed molecules decreases with strengthening adsorption interactions, which reduce the relaxation time. Intermolecular (adsorption) interactions can be described in details on study of the self-diffusion measured using pulse-gradient of the magnetic field [2-5]. These measurements demonstrate that interaction between adsorbate and adsorbent is propagated through a relatively thick layer, which can reach 2-3 nm or larger [3,6]. In aqueous suspensions of oxides, interaction of water

with solid surfaces can be detected even at 100 nm distance due to long-range component of intermolecular interaction [7], formation of the electrical double layer [8-10], and electrostatic and polarization effects [11,12].

An important parameter characterizing interaction between solids and liquids is the Gibbs free surface energy (γ_S); however, its exact measurement is difficult [13-20]. In liquid water

$$\gamma_S = \int_0^\infty \Delta G(x)dx \tag{1}$$

(where x is the thickness of the bound water layer, ΔG is the change in the Gibbs free energy dependent on x) equals to summarized changes in the Gibbs free energy of solids/water due to the existence of the interfaces. The ^{1}H NMR spectra of adsorbed water are useful and informative on the study of interfacial water, which can be frozen at T < 273K due to the impact of solid surfaces reducing the free energy of the water. The layer thickness of water unfrozen at T < 273K can be estimated using the ^{1}H NMR signal intensity measured during freezing and de-freezing processes. The interfacial water is in a quasi-liquid state at T < 273 K and characterized by a relatively narrow ^{1}H NMR signal. The signal of ice (as well as OH groups of solids) is not observed in the ^{1}H NMR spectra because a large difference in the times of cross-relaxation of protons in liquid and frozen waters.

Dependence of the unfrozen water layer thickness (i.e. the intensity I of the ^{1}H NMR signal) on temperature in aqueous suspensions or hydrated powders was studied by many authors [21-32]. It was shown that this thickness depends on the hydrophilic properties of adsorbent surfaces; for instance, it decreases as follows silica gel > kaolinite > Teflon [28]. There is a $I(T)$ hysteresis loop on freezing-de-freezing [23,31], which can appear due to overcooling of water on freezing [23]. Therefore, the $I(T)$ functions obtained on de-freezing of samples after freezing to T lower than a minimal temperature of water overcooling are more appropriate to determine the characteristics of the interfacial water. Computation of changes in the Gibbs free energy using the dependence of the signal of unfrozen water on temperature is based on the fact that the freezing temperature of the interfacial water depends on the free surface energy of adsorbent and the distance between water molecules and solid surfaces [32-35]. Condition of water freezing at the interface is the equality of the free energies of water and ice, and typically the closer the adsorbed molecules to the surfaces, the lower the temperature of water freezing.

2. CHARACTERISTICS OF THE BOUND WATER LAYERS
DETERMINED USING ^{1}H NMR

It is of interest to consider the application of this method to the aqueous suspension of fumed silica (specific surface area $S_{BET} \approx 300$ m^2/g), previously pressed ($\sim 1.14 \times 10^5$ Torr) and ball-milled. Figure 1a shows the ^{1}H NMR signal of the unfrozen water in such a suspension at different temperatures. The observed signal is linked to mobile water molecules affected by the silica surfaces. This signal is individual at the chemical shift $\delta_H \approx 4$ ppm (in respect to TMS), whose intensity decreases but half-width increases with lowering temperature in consequence of a reduction of the molecular mobility. The concentration of unfrozen water (C_{uw}) can be estimated using the signal intensity comparing with that of a given amount of water adsorbed on this oxide from the gas phase. To determine the concentration of water adsorbed on a sample (C_x), one can utilize the graph of the intensity of ^{1}H NMR signal versus the amount of water (C_a) added to the powder using a metering micropump (Figure 1b). The point of intersection of $I(C_x+C_a)$ with the X axis corresponds to the initial concentration of adsorbed water. The thickness (d) of unfrozen water (as the number of the statistical monolayers) can be computed from the concentration of adsorbed water (C_{uw}) and the specific surface area of adsorbent

$$d = 3.1 \, C_{uw}/S \tag{2}$$

Figure 2a shows the graph of the intensity of the unfrozen water signal versus temperature. Changes in the Gibbs free energy ΔG linked to lowering temperature of water freezing can be easily computed, as the thermodynamic functions of ice are known over a wide temperature range [36]. The relationship between ΔG of ice and T can be written as follows

$$\Delta G = 0.036(273 - T) \tag{3}$$

The $I(T)$ graph for the unfrozen water can be easily transformed to the dependence of ΔG for adsorbed water on the distance of the boundary between frozen and unfrozen waters to the adsorbent surface (Figure 2b).

Sometimes an increase in the intensity of the NMR signal with lowering temperature due to enhancement of nuclear level population (Curie rule [37]) should be considered. There is a relationship between the nuclear magnetization (M) of the system with N spins with the spin value s and the gyromagnetic ration g

$$M = KNg^2h^2I(s + 1)B_0/3kT \tag{4}$$

where B_0 is the magnetic field intensity, K is a constant dependent on NMR measurement conditions, h is Plank constant, k is Boltzman one. Notice that for thick water layers adsorbed on the surfaces of dispersed oxides, the choice of measurement conditions allows one to obtain the NMR signals of water (with no freezing) constant over a wide range of the temperature, i.e., the Curie rule can be ignored.
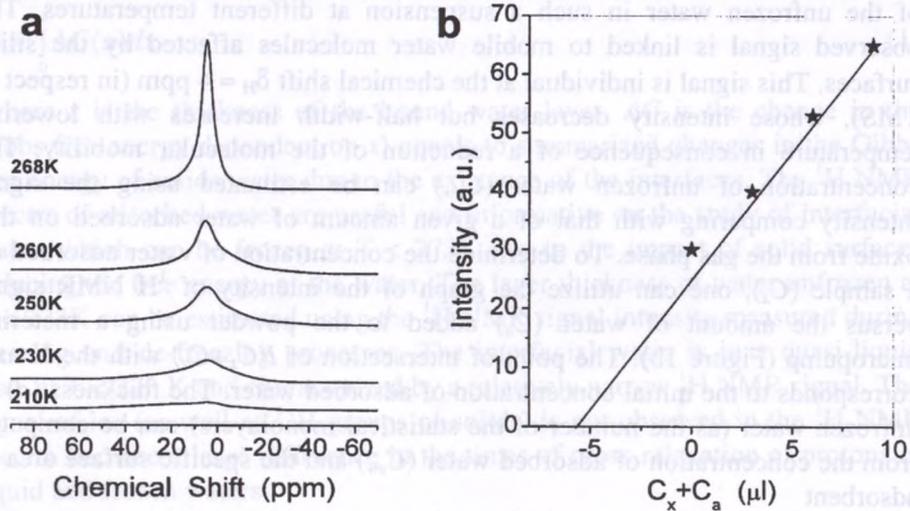
Fig. 1. (a) ^1H NMR signal of unfrozen water in aqueous suspension of fumed silica, previously pressed and ball-milled (A_p); and (b) the graph of the intensity of ^1H NMR signal versus the amount of water (C_a) added to the powder

The capillary effects in the aqueous suspensions of fumed oxides possessing nonporous primary particles are absent, and $\Delta G(C_{uw})$ determines changes in the Gibbs free energy of the interfacial water as a radial function of the unfrozen water layer thickness around spherical primary particles as C_{uw} is proportional to the layer thickness x. The value of the free surface energy of adsorbents in the aqueous suspensions can be determined using the $\Delta G(C_{uw})$ function, and Eq. (4) can be re-written as follows

$$\gamma_S = K_1 \int_0^{C_{uw}^{max}} \Delta G(C_{uw})dC_{uw} \qquad (5)$$

where K_1 is a scale coefficient, C_{uw}^{max} is the thickness of the unfrozen water layer extrapolated at $\Delta G \to 0$ (if ΔG is in kJ/mol or γ_S in mJ/m^2 that $K_1 = 55.6/S$, where S is the specific surface area of adsorbent). Two portions of the ΔG graph can be separated (Figure 2b). The first portion corresponds to a large reduction in the unfrozen water layer over a narrow ΔG range (near 273 K) and the second one is linked to small changes in the thickness over

a broad ΔG range. The first type of the interfacial water can be assigned as weakly bound water (thickness d_w) due to a long-range component of the surface forces. The second type corresponds to a greater change in the free energy (ΔG_s) over a short distance (d_s) from the surface, i.e., this is strongly bound water. The thickness of these layers (d_s and d_w for strongly and weakly bound waters) and overall changes in the free energy for them (ΔG_s and ΔG_w) can be estimated using extrapolation of the plots to the axes. In the case of a nearly linear shape of these $\Delta G(d)$ graph portions, the free surface energy at the interface of oxide/water/ice can be determined using a simple equation

$$\gamma_S = K_I(\Delta G_s d_s + \Delta G_w d_w)/2 \qquad (6)$$

This value can be computed as the sum of ΔG for all monolayers of the interfacial water

$$\gamma_S = \sum_i \Delta G_i d_i \qquad (7)$$

where ΔG_i is the average value for the i monolayer and $1 < i < d_\Sigma = d_s + d_w$. The ΔG_I value corresponds to changes in the free energy of the first monolayer. The overall ΔG_{max} value can be estimated using the $\Delta G(d)$ graph at $d \to 0$.
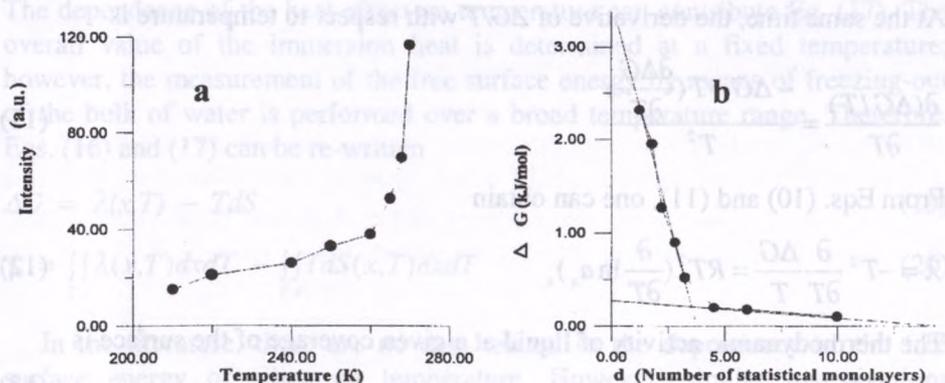
Fig. 2. (a) Dependence of the ^{1}H NMR signal intensity of unfrozen water versus temperature; and (b) dependence of variation in the free energy of water at the silica/water interface as a function of distance between the surface and the frozen/unfrozen water boundary in the aqueous suspension of A_p

3. RELATIONSHIP BETWEEN THE FREE SURFACE ENERGY γ_S
AND OTHER THERMODYNAMIC PARAMETERS

Immersion heat. The differential immersion heat λ is the heat evolved due to addition of an infinite amount of liquid onto the surface at a given

coverage x [38]. The λ value as well as ΔG characterizes the surface force field. The value $\lambda = 0$ corresponds to full compensation of the surface energy by the energy of adsorbate interaction with the surface. The λ value as well as the differential Gibbs free energy ΔG for different layers decreases farther and farther away from the surface. The differential Gibbs free energy equals to the differential work of adhesion

$$\Delta G = -W_a \tag{8}$$

The Gibbs free energy increases with increasing distance from the surface and this increment equals to a reduction of the surface Gibbs free energy of immersion. The change in the Gibbs free energy of liquid is linked with the thermodynamic activity (a_x)

$$\Delta G = -RT \ln a_x \tag{9}$$

According to the Gibbs-Helmholtz equation, the differential heat of immersion can be written as follows

$$\lambda = \partial \Delta H / \partial x = \Delta G - T(\partial \Delta G / \partial T) \tag{10}$$

At the same time, the derivative of $\Delta G/T$ with respect to temperature is

$$\frac{\partial(\Delta G/T)}{\partial T} = \frac{-\Delta G + T(\frac{\partial \Delta G}{\partial T})}{T^2} \tag{11}$$

From Eqs. (10) and (11), one can obtain

$$\lambda = -T^2 \frac{\partial}{\partial T} \frac{\Delta G}{T} = RT^2 (\frac{\partial}{\partial T} \ln a_x)_x \tag{12}$$

The thermodynamic activity of liquid at a given coverage of the surface is

$$a_x = p_x/p_s \tag{13}$$

where p_x is the pressure of saturated vapor over the interface liquid at coverage x, p_s is the pressure of saturated vapour over the pristine liquid. Using Eq. (10) one can obtain

$$\lambda = RT^2(\partial \ln p_x/\partial T)_x - RT^2(\partial \ln p_s/\partial T) \tag{14}$$

where the first term in the right part is the liquefaction heat Q_x of the vapor on the surface of the liquid, the second one is the liquefaction heat (Q_0) under standard conditions, then

$$\lambda = Q_x - Q_0 \tag{15}$$

Consequently, the differential heat of immersion equals to the difference between the liquefaction heats of the water vapour over the adsorbent surface and the bulk water. Thus, there is a similarity between the determination of the immersion heat in Eq. (15) and ΔG described above. Both the immersion heat and differential free energy are determined by the difference in the thermodynamic functions for the phase transfer to free and interfacial liquids. Since the free energy and enthalpy are linked by equation

$$\Delta G = \lambda - T\Delta S \tag{16}$$

which can be re-written for overall values of the free surface energy and summary heat of immersion (λ_i) with consideration of changes in the thermodynamic functions over the total thickness of the bound water layer

$$\gamma_s = \lambda_i - \int_x T\Delta S(x)dx \tag{17}$$

and

$$\lambda_i = \int_x \lambda dx \tag{18}$$

The dependence of the heat effect on temperature can contribute Eq. (17). The overall value of the immersion heat is determined at a fixed temperature; however, the measurement of the free surface energy by means of freezing-out of the bulk of water is performed over a broad temperature range. Therefore, Eqs. (16) and (17) can be re-written

$$\Delta G = \lambda(x,T) - TdS \tag{19}$$

$$\gamma_s = \int_T\int_x \lambda(x,T)dxdT - \int_T\int_x TdS(x,T)dxdT \tag{20}$$

In the literature, there are no data related to the dependence of the free surface energy of silica on temperature. However, similar investigations performed by means of inverse gas chromatography (IGC) for graphite [18] show that a dispersion component of γ_s decreases from 140 mJ/m^2 to 125 mJ/m^2 with elevating temperature from 300 K to 360 K. One can assume that similar small changes in γ_s can occur in the case of dispersed oxides. Then non-isothermicity of freezing-out of the bulk water under the ^{1}H NMR measurements does not give large errors in respect to γ_s, which can be compared with the free surface energy determined using other methods.

Disjoining pressure and surface forces. One of frequently used characteristics of the surface forces is the disjoining pressure, which is the

difference between the pressure p_l on the liquid layer located between two solid surfaces and the pressure p_0 in the bulk of liquid [7]

$$\Pi(x) = p_l - p_0 \tag{21}$$

where x is the thickness of the liquid layer. Besides, the disjoining pressure equals to changes in the Gibbs free energy over the unit distance to the surface at constant temperature (T), pressure (p) and chemical potential (μ)

$$\Pi(x) = -(dG/dx)_{TP\mu} \tag{22}$$

Typically the disjoining pressure is measured using direct methods to determine the force needed for closing two plates in liquid media and these methods are described in detail elsewhere [7,8]. Formally, the disjoining pressure value can be estimated from the data shown in Figure 2b. However, Eq. (22) corresponds to the determination of the Π value at a constant temperature. Therefore for isobaric freezing-out of the bulk liquid, one can use an effective value of surface forces, which can be calculated using the relationship

$$F = (\Delta G \, m)/x \tag{23}$$

where m is the mass of unfrozen water in moles, x is the distance to the surface. If the ΔG value is in kJ/mol, C_{uw} in mg/g, x in nm, then

$$F = \frac{\Delta G C_{uw} \cdot 10^9}{18x} \, \text{(N/g)} \tag{24}$$

The derivative value of ΔG with respect to the thickness of the bound water layer (x) or the concentration of unfrozen water

$$\theta = d(\Delta G)/dx \, ; \quad \text{or} \quad \theta = d(\Delta G)/d(C_{uw}) \tag{25}$$

Maxima of this dependence determine the characteristic distances to the surface (or concentration of bound water), for which changes in the type of surface forces are observed. For fumed silica pressed at $p = 150$ bar, the dependences $\theta = f(x)$ and $F = f(x)$ are shown in Figure 3, where F is in GN per gram of adsorbent and shows the interaction force between liquid water and gram of silica. This value divided by the specific surface area corresponds to the adhesion force per unit of the surface area. In the case of direct measurements, the force between two plates in liquid water is estimated [39-43], but in our measurements, the adhesion force value is computed as the interaction force between the solid surface and liquid medium. These forces are the main characteristic of many parameters studied for composites and filled matters. One can separate long-range and short-range components in the adhesion forces for the aqueous suspension of fumed silica (Figure 3). This suggests the

possibility of the determination of strongly and weakly bound waters. Change in the type of the surface forces occurs at mean distance to the surface of approximately 1 nm.
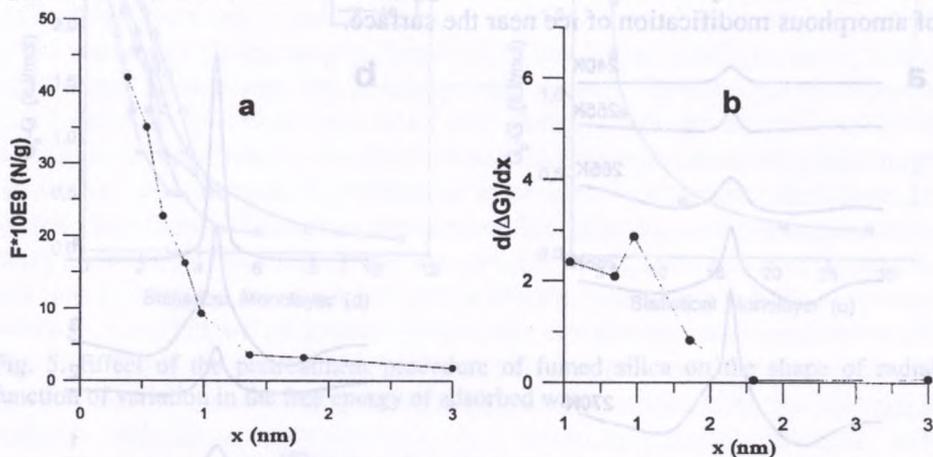
Fig. 3. Radial dependencies of (a) adhesion forces and (b) $\theta(x)$ value for A_p aqueous suspension

4. HIGHLY DISPERSE OXIDES

4.1. Influence of the adsorbent pretreatment on adhesion forces. The samples of fumed silica A-300 (Pilot Plant of the Institute of Surface Chemistry, Kalush, Ukraine; specific surface area $S_{BET} \approx 300$ m^2/g, apparent density $C_b \approx 40$ mg/cm^3) were studied such as non-treated (A_{nt}), heated at 520 K for 3 h (A_h), wetted with water (A_w) or hexane (supplied by Aldrich) (A_{hex}) then dried at 293 K ($C_b = 90$ mg/cm^3), pressed at 15 MPa, ($C_b = 250$ mg/cm^3), (A_p) [44,45].

Changes in the ^{1}H NMR spectra as functions of the temperature and the silica concentration for the frozen suspension of A_{nt} are given in Figures 4a and 4b, respectively. The spectrum of water adsorbed on A_p (Figure 1a) has a single signal, whose width increases while the temperature goes down due to a decline in the molecular mobility of adsorbed water and the intensity falls as the thickness of region aqueous close to the silica surface decreases through freezing. The same type of temperature dependent changes is observed in the spectra registered for A_w and A_{hex}. The signal of adsorbed water for A_h and A_{nt} is observed againts the background of a considerably wider signal having a shape different from the Gaussian one. Because of their similarity only the spectra for water on A_h are given. The intensity of a broad component quickly falls as a function of decrease in temperature, and it is not observed in the

spectra at T < 255 K (Figure 4). It has been shown earlier [46,47] that the broad component of the signal for water diminishes with decrease in the distance between the silica particles. It has been suggested that it is due to the formation of amorphous modification of ice near the surface.
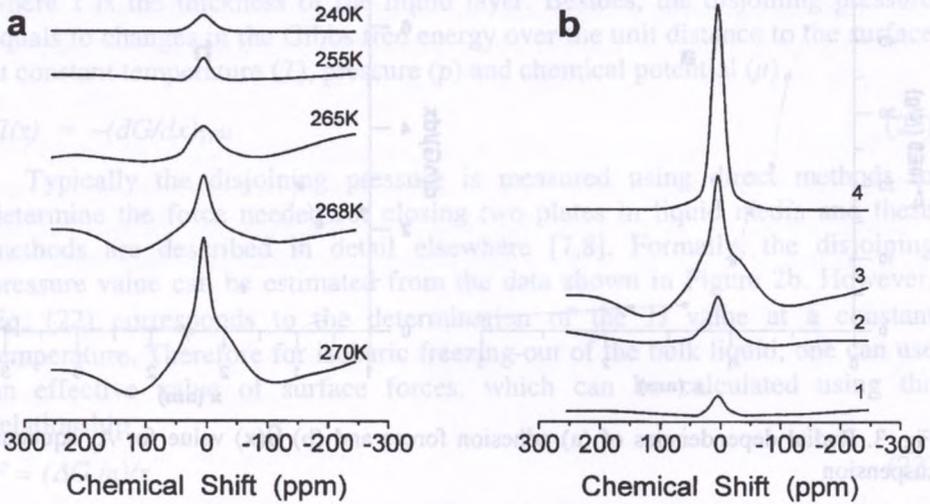
Fig. 4. Dependencies of ^1H NMR spectra of water in frozen aqueous suspensions of fumed silica A_{nt} on (a) temperature and (b) silica concentration: 1 % w/w (1); 2 % w/w (2); 6 % w/w (3); and 20 % w/w (4)

Figures 5 and 6 show the $\Delta G(d)$ and $F(x)$ graphs for silicas differently pre-treated. These graphs reflect the type of the radial functions relating to changes in the free energy of water in the adsorption layer. Two segments may be revealed on the dependencies obtained: the segment of a quick decrease in the thickness of the unfrozen water layer in a narrow range of the ΔG value changes (temperature is about 273 K) and the one, where d decreases relatively weakly in a broad range of changes in the ΔG values. As was shown in section 2, there are weakly and strongly bonded waters respectively. The total value of the free energy of the adsorbed water using linear dependences $\Delta G_s(d)$ and $\Delta G_w(d)$ may be defined according to Eq. (5). The ΔG values calculated using data shown in Figure 6 are summarized in Table 1.

a

b
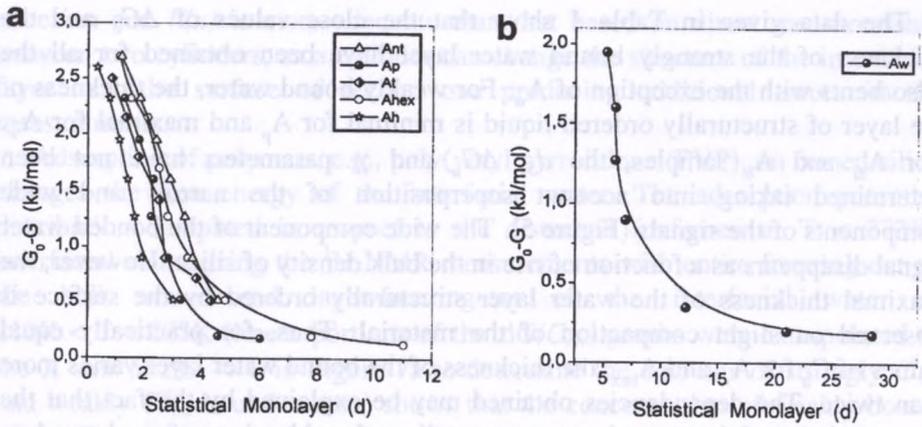
Fig. 5. Effect of the pretreatment procedure of fumed silica on the shape of radial function of variation in the free energy of adsorbed water
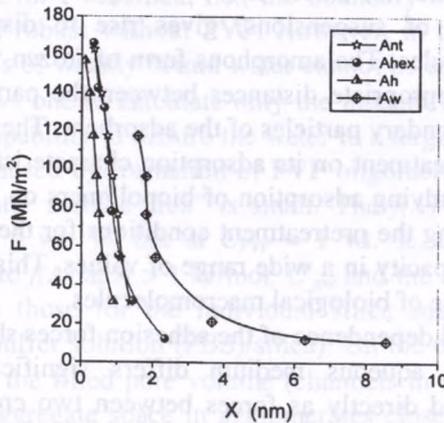
Fig. 6. Effect of adsorbent pretreatments on the radial function of adhesion forces for aqueous suspensions of fumed silica

Tab. 1. Influence of silica pretreatment on the characteristics of the interfacial water

Material	ΔG_s kJ/mol	ΔG_w kJ/mol	d_s	d_w	γ_S mJ/m^2
A_{nt}	3.4	–	5	–	–
A_{hex}	3.5	0.35	4.5	17	195
A_p	3.8	0.35	3.2	13	160
A_h	3.3	–	4.0	–	–
A_t	2.9	–	2.7	–	–
A_w	5.3	0.50	8.0	35	540

Note. Unfrozen water layer thickness d are shown in statistical monolayers.

The data given in Table 1 show that the close values of ΔG_S and the thickness of the strongly bound water layer have been obtained for all the adsorbents with the exception of A_w, For weakly bound water, the thickness of the layer of structurally ordered liquid is minimal for A_p and maximal for A_w. For A_{nt} and A_h samples, the d_S, ΔG_w and γ_S parameters have not been determined taking into account superposition of the narrow and wide components of the signals (Figure 5). The wide component of the bonded water signal disappears as a function of rise in the bulk density of silica. However, the maximal thickness of the water layer structurally ordered by the surface is observed on slight compaction of the material. Thus, for practically equal values of C_b for A_w and A_{hex}, the thickness of the bound water layer varies more than twice. The dependencies obtained may be explained by the fact that the characteristics of the water layers structurally ordered by the surface depend on interparticle interactions. Fumed silica particles in the aqueous suspensions are present in the form of aggregates (100-500 nm) and agglomerates (> 1 μm) [48]. These swarms are not stable and even exposure to negligible external factors (e.g. shaking of suspensions) gives rise to dispersion as well to amalgamation of particles. The amorphous form of frozen water is likely to be formed only at the appropriate distances between the particles and favorable dimensions of the secondary particles of the adsorbent. Therefore, the influence of the adsorbent pretreatment on its adsorption characteristics should be taken into account while studying adsorption of biopolymers on dispersed materials. By means of modifying the pretreatment conditions for the adsorbent one may vary its adsorption capacity in a wide range of values. This will have an effect on the adsorption value of biological macromolecules.

The shape of radial dependence of the adhesion forces shown in Figure 6 for fumed silica in the aqueous medium differs significantly from similar dependences measured directly as forces between two crossed cylinders [49--51]. Clearly from these results (Figure 6), the adhesion force value decreases practically linearly with the distance (not far from the surface). At the same time, the interaction force between two cylinders changes in the sign at a short distance between them due to too much decrease in the liquid layer thickness and can be described as follows $F = x^{-n}$. When x is smaller than the adsorbed layer the work is made against the adsorption forces; and the structure of this layer is destroyed. In the experiments on freezing-out of the bulk phase, the adhesion force $F = dG/dx$ can be determined as $\Delta G/x$ (where x is the distance between the surface and the outer boundary of the unfrozen water layer). While the energy of interaction between the oxide surface and adsorbed water molecules typically increases with decreasing number of molecules in the interfacial layer, change in the sign of F is not observed. One can assume that such a method (however, as an indirect one) to estimate the work of forces of

adhesion and $F(x)$ is more adequate than that based on direct measurements between two cylinders, as a cylinder can change the structure of the interfacial layer near the surface of second one producing additional errors in the measurements.

Adsorption of polymers, e.g., poly(vinyl pyrrolidone (PVP), on fumed silica changes the free energy of the interfacial water. The adsorption potential distribution computed in respect to the disturbed (unfrozen at T < 273K) interfacial water using the ^{1}H NMR measurements with entire freezing-out of the bulk water and layer-freezing-out of the interfacial water at 210K < T < 273K (linear portions of the $\Delta G(C_{uw})$ graphs were extrapolated to the X axis at $\Delta G \rightarrow 0$ in Figure 7a to determine the amounts of strongly C^s_{uw} and weakly C^w_{uw} bound waters) shows that the concentration of weakly bound water (Figure 7b, A < 1 kJ/mol) are lower for the pure silica suspension or the pure PVP solution. The decline in a linear portion of the $\Delta G(C_{uw})$ graph at small ΔG (Figure 7a) corresponding to weakly bound water is larger for pure silica suspension than that for PVP/silica; i.e., the boundary between disturbed and bulk waters is more robust without PVP. However, in the case of pure PVP solution, the amounts of weakly bound water cannot be estimated, while nearly linear $\Delta G(C_{uw})$ allows one to calculate only the amount of the strongly bound water, as the PVP capability to disturb the water to a large distance is low. This effect can be also caused by formation of PVP oligomers in the pure aqueous solution, whose "outer surface area" is small. The $f(A)$ intensity (Figure 7b) increases at $C_{PVP} = 5$ wt. %, but at $C_{PVP} = 1$ wt. %, the opposite effect is observed in respect to $f(A)$ at A > 1 kJ/mol, C^s_{uw} and the free surface energy γ_S in comparison with those for the individual silica suspension (or C^s_{uw} for PVP/physiological buffer solution (PBS)/silica). On the other hand, changes in ΔG as a function of the filled pore volume (channels in aggregates of primary particles and inter-aggregate space in agglomerates close to the outer surfaces of aggregates) (Figure 7c) and the pore radius (Figure 7d) show that the silica impact on water in pores at R_p between 1 and 10 nm is significantly larger (as the free energy is lower) than that for the PVP/silica suspension ($C_{PVP} = 1$ wt. %, $\gamma = C_{PVP}/C_{SiO2} \approx 0.17$) due to reduction in long-range components of surface forces for silica particle swarms rearranged and shielded by PVP molecules. Clearly, in the case of large mesopores, unfrozen water can be located close to the silica particles, e.g., the outer surfaces of aggregates. These effects can be explained by formation of a denser PVP layer at the silica surfaces at low PVP concentrations ($\gamma < 0.2$) resulting in the decrease in the amount of water strongly bound to the oxide surfaces. At large $C_{PVP} = 5$ wt. % ($\gamma \approx 0.83$), a major portion of PVP is in the non-immobilized state or weakly interacts with the silica surfaces, but the amount of water weakly and strongly bound to PVP molecules increases significantly (Figure 7a). Thus, at $\gamma < 0.2$, polymer

molecules adsorb strongly and the number of free pyrrolidone groups can be less than bonded ones (at $\gamma \approx 0.2$, the relative number of free C=O groups in PVP adsorbed on silica from solution and then dried at room temperature is approximately 2/3, according to IR spectra); i.e., the adsorbed PVP layer is relatively dense, and oxide particles or PVP molecules can disturb only a relatively thin interfacial water layer. At great C_{PVP}, a significant portion of PVP molecules has free tails, which do not interact with the silica surfaces but effectively interact with water molecules, whose great portion is disturbed by polymer molecules. However, a decline in the ΔG dependence on C_{uw}, V_p or R_p (especially at $\Delta G > -0.7$ kJ/mol) is small for a relatively thick layer of weakly bound water (Figure 7).
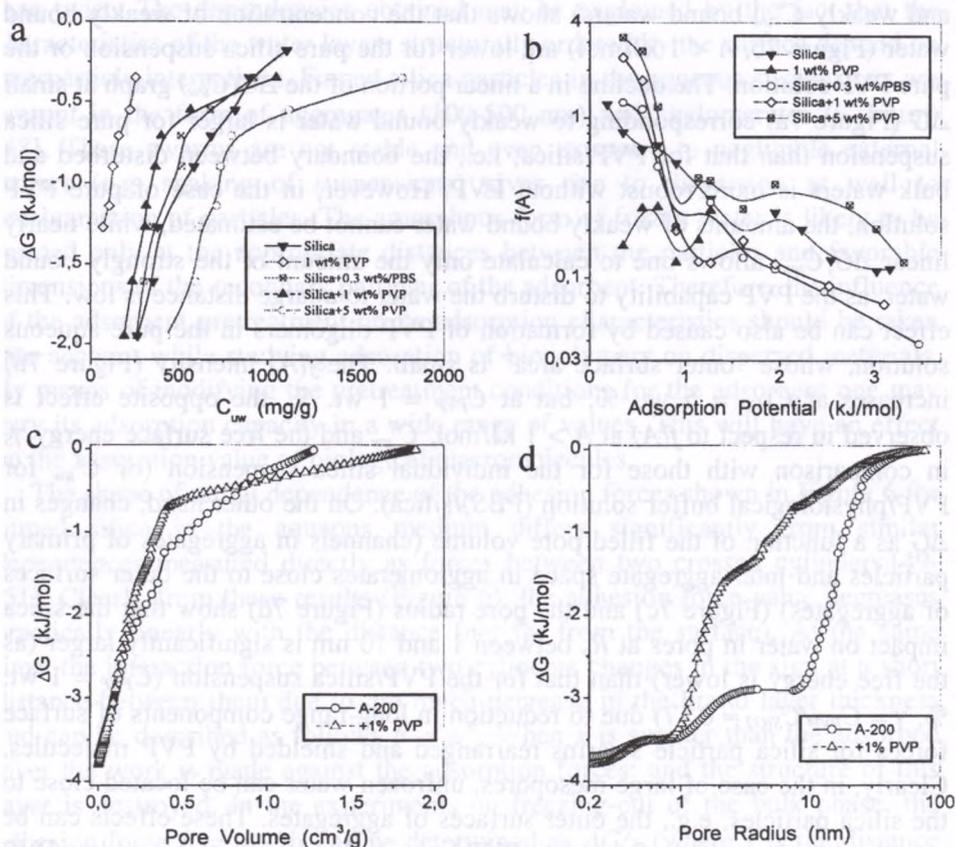
Fig. 7. (a, c, d) Changes in the free energy and (b) water adsorption potential distributions for pure PVP solution and suspensions of silica, silica/PVP, and silica/PVP/PBS computed on the basis of ^{1}H NMR data; ΔG as a function of (c) filled pore volume and (d) pore radius for silica (6 wt. % A-200) and PVP/silica (1 wt. % PVP, 6 wt. % A-200) suspensions

4.2. Modified silica and mixed oxides. Mixed oxides are promised materials to utilize them as catalysts, polymer fillers, and adsorbents possessing surface Brönsted and Lewis acid sites [52-56]. Besides this, disperse particles of dust pollutants of industrial and natural origins are mostly the mixture of porous and non-porous oxides SiO_2, Al_2O_3, TiO_2, etc., containing carbon deposits on the surface, or chemisorbed molecules of organic compounds. In atmosphere, these particles serve as nuclei of condensation or crystallization for water vapour.

In Figure 8, there are shown the dependencies of changes in the free energy versus the concentration of unfrozen water. The characteristics of the layers of water adsorbed on the surface of the studied samples and the free surface energy values calculated using Eq. (5) are represented in Table 2.
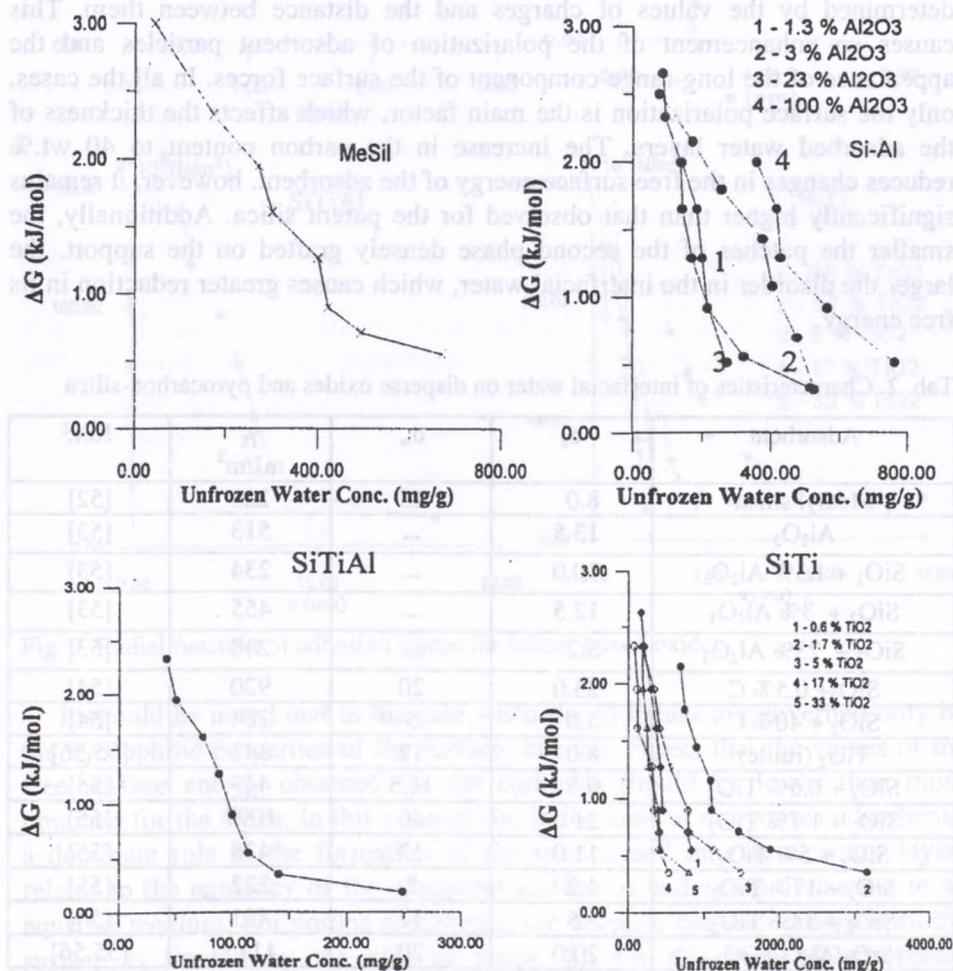
Fig. 8. Dependence of changes in the free energy of the interfacial water for fumed mixed oxides as a function of the unfrozen water concentration

It follows from Table 2 that for alumina-silica we have average value of the surface free energy between values corresponding individual oxides. For non-porous materials with a low surface concentration of alternate compounds (pyrocarbon on SiO_2; SiO_2/Al_2O_3 on TiO_2), we have a maximal value of the surface free energy. The most probable explanation of this fact is the polarization of the adsorbent surface caused by charge exchange between different phases. As was shown by Dukhin [12], upon the appearance of differently charged areas on the surface of disperse particles, there is a long-range component of the surface forces, which caused by the electrostatic field directed along the surface of particles. In this field, the dipoles of water molecules are under orientation effect. Remoteness of this type of interaction is determined by the values of charges and the distance between them. This causes en enhancement of the polarization of adsorbent particles and the appearance of the long-range component of the surface forces. In all the cases, only the surface polarization is the main factor, which affects the thickness of the adsorbed water layers. The increase in the carbon content to 40 wt.% reduces changes in the free surface energy of the adsorbent, however, it remains significantly higher than that observed for the parent silica. Additionally, the smaller the patches of the second phase densely grafted on the support, the larger the disorder in the interfacial water, which causes greater reduction in its free energy.

Tab. 2. Characteristics of interfacial water on disperse oxides and pyrocarbon-silica

Adsorbent	d_s	d_w	γ_s mJ/m^2	Ref.
Methyl silica	8.0	15	220	[52]
Al_2O_3	13.5	–	513	[53]
SiO_2 + 1.3% Al_2O_3	10.0	–	234	[53]
SiO_2 + 3% Al_2O_3	12.5	–	455	[53]
SiO_2 + 23% Al_2O_3	5.2	–	248	[53]
SiO_2 + 0.5% C	25.0	20	920	[54]
SiO_2 + 40% C	5.0	5	284	[54]
TiO_2 (rutile)	8.0	12	341	[55,56]
SiO_2 + 0.6% TiO_2	9.5	11.5	449	[55]
SiO_2 + 1.7% TiO_2	21.0	40	1097	[55]
SiO_2 + 5% TiO_2	11.0	13	428	[55]
SiO_2 + 17% TiO_2	4.2	5	222	[55]
SiO_2 + 33% TiO_2	7.5	17	421	[55]
$SiO_2/Al_2O_3/TiO_2$	20.0	20	1113	[55,56]

Note. Unfrozen water layer thickness d are shown in statistical monolayers
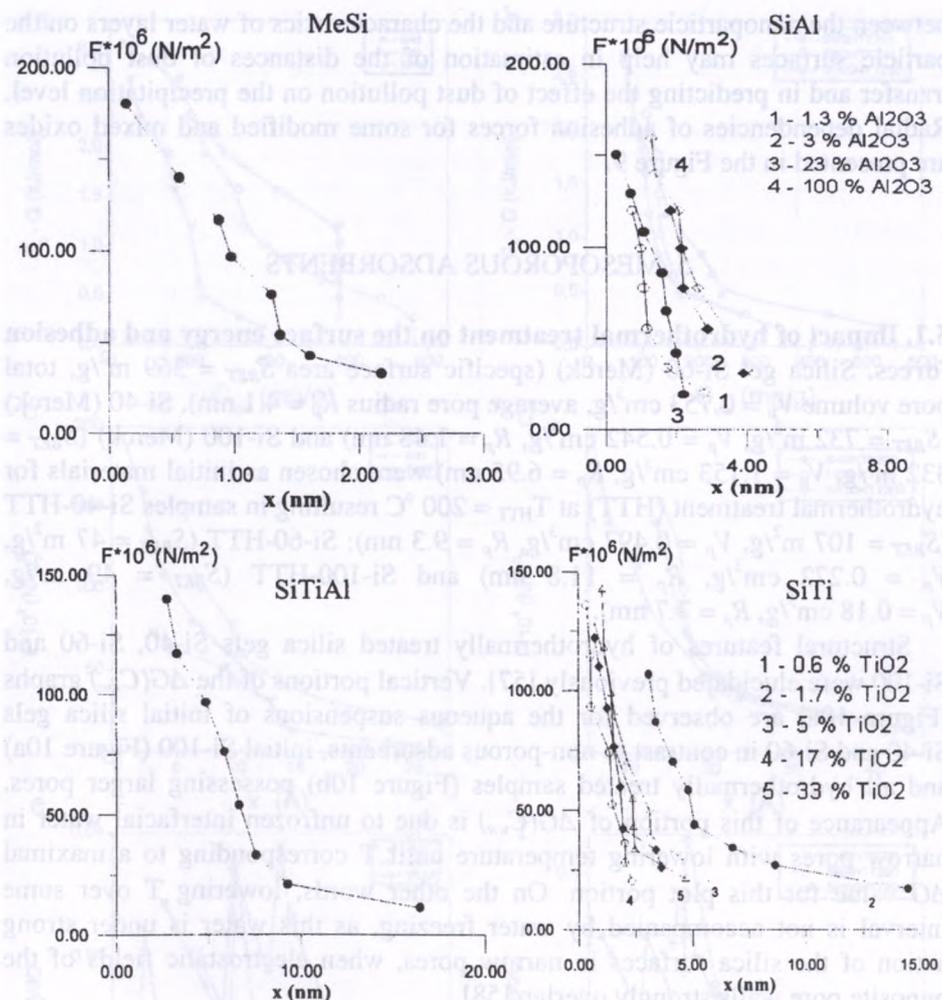
Fig. 9. Radial function of adhesion forces for fumed mixed oxides

It should be noted that in the case when the γ_S values are governed only by the hydrophilic properties of the surface, one can expect that the values of the free surface energy obtained for the carbosils should be lower than those obtained for the silica. In this connection, in the case of nonporous adsorbents, a dominant role in the formation of the structurized interfacial water layers relates to the tendency of the adsorbent surface to undergo polarization in an aqueous medium. For porous adsorbents, the distance between chargers on the surface is limited by the size of pores. So for this type of adsorbents polarization effects are insignificant and interaction with the aqueous medium is governed by the hydrophilic properties of the samples. The correlation

between the nanoparticle structure and the characteristics of water layers on the particle surfaces may help in estimation of the distances of dust pollution transfer and in predicting the effect of dust pollution on the precipitation level. Radial dependencies of adhesion forces for some modified and mixed oxides are presented in the Figure 9.

5. MESOPOROUS ADSORBENTS

5.1. Impact of hydrothermal treatment on the surface energy and adhesion forces. Silica gel Si-60 (Merck) (specific surface area S_{BET} = 369 m^2/g, total pore volume V_p = 0.753 cm^3/g, average pore radius R_p = 4.1 nm), Si-40 (Merck) (S_{BET} = 732 m^2/g, V_p = 0.542 cm^3/g, R_p = 1.48 nm) and Si-100 (Merck) (S_{BET} = 332 m^2/g, V_p = 1.153 cm^3/g, R_p = 6.95 nm) were chosen as initial materials for hydrothermal treatment (HTT) at T_{HTT} = 200 °C resulting in samples Si-40-HTT (S_{BET} = 107 m^2/g, V_p = 0.497 cm^3/g, R_p = 9.3 nm); Si-60-HTT (S_{BET} = 47 m^2/g, V_p = 0.272 cm^3/g, R_p = 11.8 nm) and Si-100-HTT (S_{BET} = 49 m^2/g, V_p = 0.18 cm^3/g, R_p = 7.7 nm).

Structural features of hydrothermally treated silica gels Si-40, Si-60 and Si-100 were elucidated previously [57]. Vertical portions of the $\Delta G(C_{uw})$ graphs (Figure 10a) are observed for the aqueous suspensions of initial silica gels Si-40 and Si-60 in contrast to non-porous adsorbents, initial Si-100 (Figure 10a) and all hydrothermally treated samples (Figure 10b) possessing larger pores. Appearance of this portion of $\Delta G(C_{uw})$ is due to unfrozen interfacial water in narrow pores with lowering temperature until T corresponding to a maximal ΔG value for this plot portion. On the other words, lowering T over some interval is not accompanied by water freezing, as this water is under strong action of the silica surfaces in narrow pores, when electrostatic fields of the opposite pore walls strongly overlap [58].

The concentration of strongly bound water C^s_{uw} decreases with increasing pore size both for initial and hydrothermally treated silica gels (Table 3). The concentration of weakly bound water C^w_{uw} is larger for the HTT samples due to the enhancement of the pore size; however, the relationships between the C^w_{uw} values for different silica gels (initial and HTT) more complex than those for C_{uw} (Table 3). Notice that the volume of unfrozen water ($C^w_{uw} + C^s_{uw}$) for HTT-200 samples is larger than their pore volume, maybe due to formation of thick water layers on the outer surfaces of treated samples. Also, filling of large pores by nitrogen could be incomplete at $p/p_0 \approx 0.98$ (used to estimate V_p) in contrast to filling by water in the aqueous suspensions.
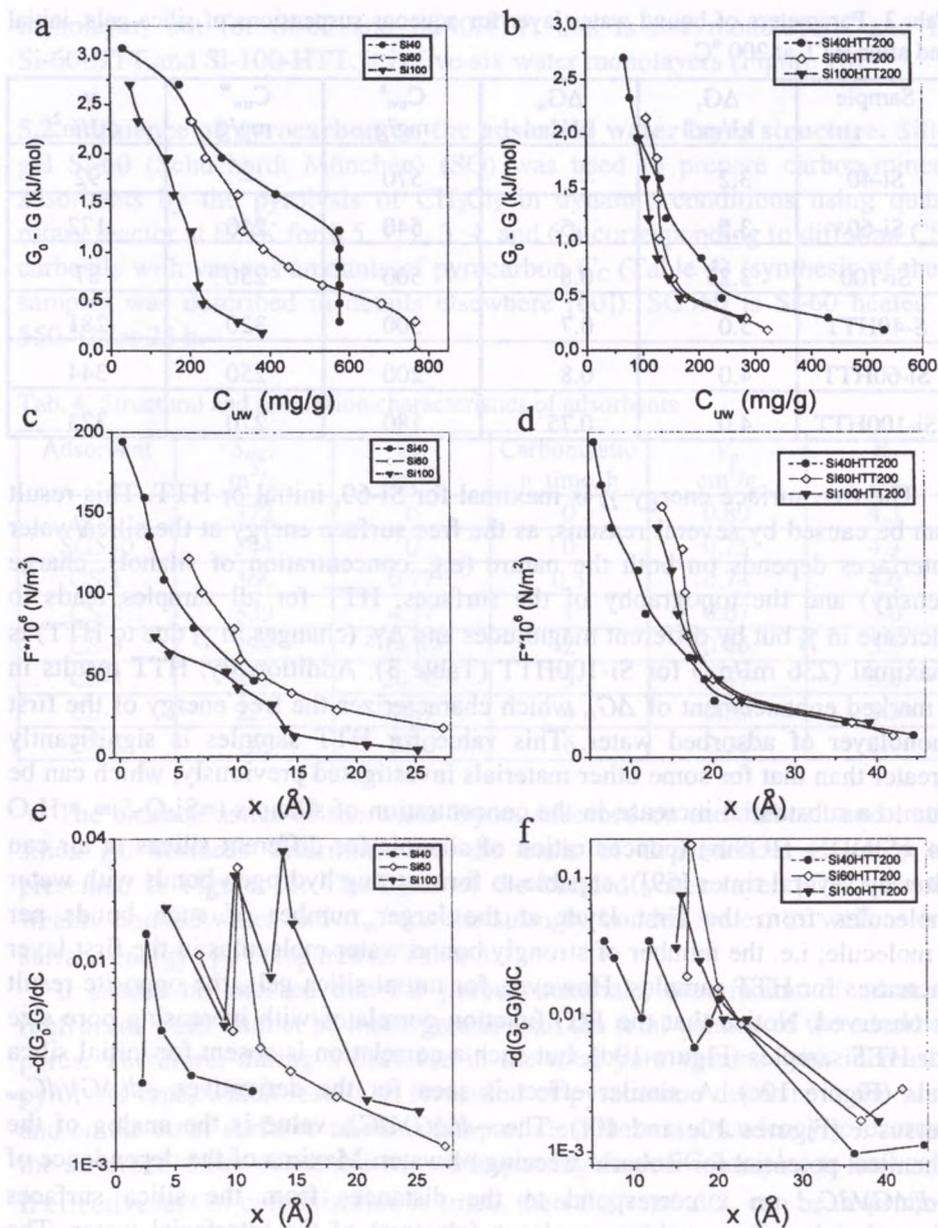
Fig. 10. Changes in the Gibbs free energy of the interfacial water in the aqueous suspensions of (a) initial and (b) hydrothermally treated Si-40, Si-60, and Si-100; and corresponding (c, d) adhesion forces and (e, f) derivatives $d(\Delta G)/dC_{uw}$ as functions of the distance x (in Å) from the silica surface

Tab. 3. Parameters of bound water layer for aqueous suspensions of silica gels, initial and after HTT at 200 °C

Sample	ΔG_s kJ/mol	ΔG_w kJ/mol	C_{uw}^s mg/g	C_{uw}^w mg/g	γ_S mJ/m^2
Si-40	3.2	–	570	–	92
Si-60	3.5	1.5	540	210	172
Si-100	3.25	0.8	500	250	87
S-40HTT	5.0	0.7	300	320	281
Si-60HTT	4.0	0.8	200	250	344
Si-100HTT	4.0	0.75	180	270	323

The free surface energy γ_S is maximal for Si-60, initial or HTT. This result can be caused by several reasons, as the free surface energy at the silica/water interfaces depends on both the nature (e.g. concentration of silanols, charge density) and the topography of the surfaces. HTT for all samples leads to increase in γ_S but by different magnitudes and $\Delta\gamma_S$ (changes in γ_S due to HTT) is maximal (236 mJ/m^2) for Si-100HTT (Table 3). Additionally, HTT results in a marked enhancement of ΔG_s, which characterizes the free energy of the first monolayer of adsorbed water. This value for HTT samples is significantly greater than that for some other materials investigated previously, which can be due to a substantial increase in the concentration of silanols ($\equiv$Si-O-Si$\equiv$ + H$_2$O $\rightarrow$ $\equiv$SiOH + HOSi$\equiv$) (concentration of silanols for different silicas in air can alter by several times [59]), capable to form strong hydrogen bonds with water molecules from the first layer at the larger number of such bonds per a molecule; i.e. the number of strongly bound water molecules in the first layer increases for HTT samples. However, for initial silica gels, the opposite result is observed. Notice that the $F(x)$ function correlates with increasing pore size for HTT samples (Figure 10d), but such a correlation is absent for initial silica gels (Figure 10c). A similar effect is seen for the derivatives $-d(\Delta G)/dC_{uw}$ versus x (Figures 10e and 10f). The $-d(\Delta G)/dC_{uw}$ value is the analog of the chemical potential for isobaric freezing of water. Maxima of the dependence of $-d(\Delta G)/dC_{uw}$ on x correspond to the distances from the silica surfaces characterizing more stable complexes (clusters) of the interfacial water. The position of these maxima shifts toward larger x with increasing pore size for both initial and HTT silicas (for HTT samples, the x values were computed in a model of a flat surface). These effects can be explained by the significant differences in the unfrozen water layers dependent on the pore size. It should be noted that for Si-40, the $-d(\Delta G)/dC_{uw}$ maximum corresponds to a water

monolayer, but for Si-60 and Si-40HTT, this is 3-4 monolayers, and for Si-60-HTT and Si-100-HTT, it is five-six water monolayers (Figure 10).

5.2. Influence of pyrocarbon on the adsorbed water layer structure. Silica gel Si-60 (Schuchardt München) (SG) was used to prepare carbon-mineral adsorbents by the pyrolysis of CH_2Cl_2 in dynamic conditions using quartz rotary reactor at 823K for 0.5, 1, 2, 3, 4, and 6 h corresponding to different CS-i carbosils with various amounts of pyrocarbon C_C (Table 4) (synthesis of these samples was described in details elsewhere [60]). SG550 is Si-60 heated at 550 °C for 24 h.

Tab. 4. Structural and adsorption characteristics of adsorbents

Adsorbent	S_{BET} m²/g	C_C wt.%	Carbonizatio n time, h	V_p cm³/g	R_p nm
SG	372	0	0	0.80	4.3
SG550	344	0	0	0.75	4.4
CS-1	366	0.77	0.5	0.74	4.0
CS-2	339	4.37	1	0.67	4.0
CS-3	299	14.89	2	0.56	3.8
CS-4	259	20.32	3	0.47	3.6
CS-5	223	26.7	4	0.39	3.5
CS-6	163	35.0	6	0.28	3.4

The characteristics of the water layers adsorbed on the carbosil and initial silica gel surfaces determined on the basis of dependences $\Delta G(C_{uw})$ are presented in Figure 11. Thickness of the bonded water layer (C_{uw}^w) for the weakly bonded water and C_{uw}^s for the strongly bonded water) as well as free surface energy (γ_S) compared in Table 5.

It should be stressed that for porous materials, the amount of adsorbed (unfrozen) water cannot be much greater than the total volume of the adsorbent pores. Therefore, during a decrease in the total pore volume with increasing pyrolysis time, which results in formation of pyrocarbon deposits in the pores and on the outer surfaces of silica gel particles, there is a tendency to decrease the adsorbed water concentration while passing from SG samples to carbosils. If effectiveness of carbonization is small, then C_{uw}^w and ΔG_w can be determined quite adequately, but in case of other samples, they have a form of approximation. Appearance of inflections on the $\Delta G(C_{uw})$ graphs can be caused by the heterogeneity of the adsorbent surfaces and limitation of the pore volume.
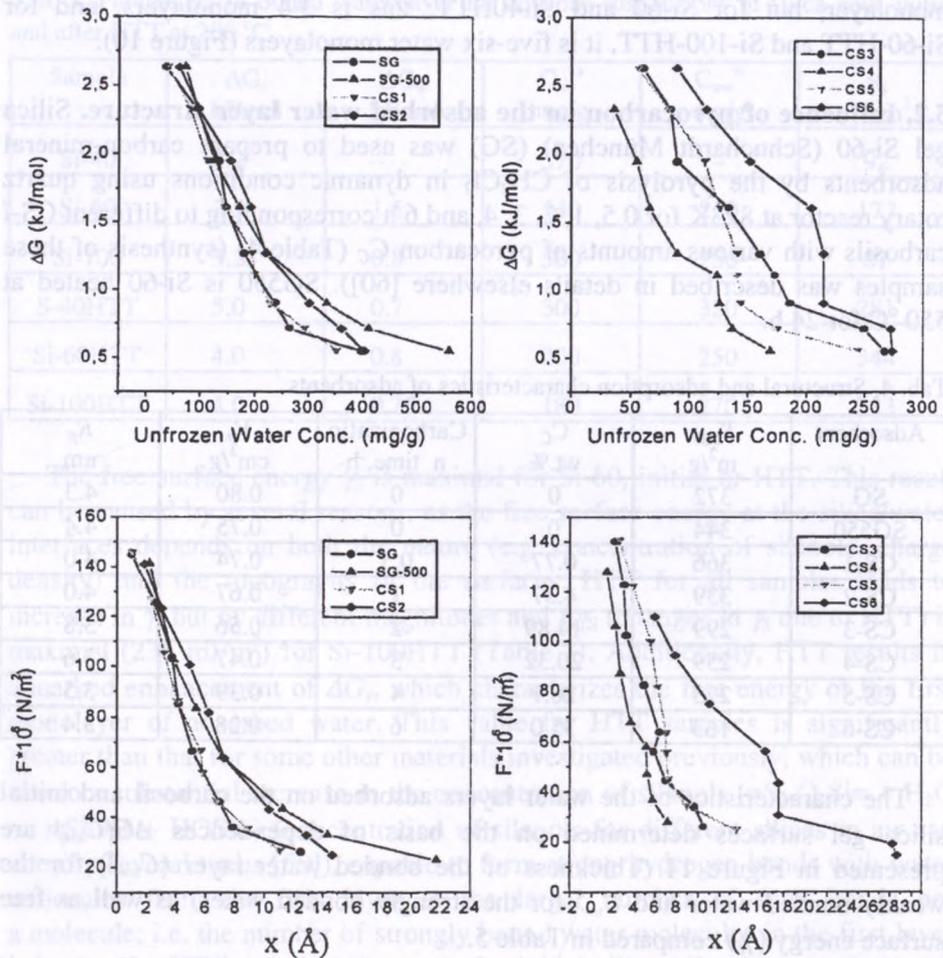
Fig. 11. Changes in the Gibbs free energy of the interfacial water in the aqueous suspensions of initial silica gel and mesoporous carbosils and radial function of adhesion forces for these adsorbents

Hydration properties of the adsorbent surfaces at the adsorbent/water interface can be expressed the most completely through the surface free energy. It follows from the data in Table 5, that γ_S increases as a result of silica gel thermally treatment from 115 mJ/m^2 to 150 mJ/m^2. The initial stage of silica surface carbonization causes a decrease in the free surface energy whereby γ_S decreases to 72 mJ/m^2 for CS-4. It is in agreement with the statement that the surface hydration properties are determined by the concentration of surface silanols, which can form the strong hydrogen bonds with water molecules. Adsorption sites for water on pyrocarbon deposits are oxidized carbon atoms,

whose concentration is much smaller than that of SiOH groups on the silica surface; therefore carbon deposits should weaken the hydrophilic properties of the hybrid adsorbents. However, it is stated that there is an increase in the adsorbent hydrophilic properties for the samples CS-5 and CS-6, which is evident in the increase of the values γ_S and C^s_{uw} and for CS-6, γ_S is even higher than that for the initial silica.

Tab. 5. Characteristics of water adsorption layers from the ^1H NMR data on the surface of mesoporous carbosils

Adsorbent	ΔG_s kJ/mol	$C_{uw}{}^s$ mg/g	ΔG_w kJ/mol	$C_{uw}{}^w$ mg/g	γ_S mJ/m^2
SG	2.8	330	1	520	115
SG550	3.5	270	1.2	730	150
CS1	3.0	320	1.5	230	110
CS2	3.2	375	2.2	155	132
CS3	4.0	175	1.7	225	109
CS4	3.0	150	1.4	125	72
CS5	3.5	220	1.2	250	139
CS6	3.7	300	1.8	100	240

6. MICROPOROUS MATERIALS

6.1. Activated carbons. Carbon adsorbent PS-0 produced utilizing plum stones (Wood Dry Distillation Works, Hajnówka, Poland) was used as the initial material. PS-0 was subjected to hydrothermal modification (HTM) in a stainless steel autoclave (0.3 dm^3). To prepare oxidized adsorbents PS-OX1 and PS-OX2, 5 g of PS-0 was placed in a quartz thimble to the autoclave with 20 cm^3 of 30 % H$_2$O$_2$ and treated in the vapour phase at 523 K (PS-OX1) or 623 K (PS-OX2) for 6 h. A reduced adsorbent (PS-H) was prepared on heating of PS-0 in a H$_2$ stream in a quartz flow reactor at 1073 K for 8 h [61].

Figure 12 shows variations in the free Gibbs energy as a function of the concentration of unfrozen water in the aqueous suspensions of the initial (curve 1), reduced (curve 2), and oxidized carbons (curves 3 and 4). The $\Delta G(C_{uw})$ graphs exhibit the portions of the unfrozen water, which remain near constant over a wide ΔG range. This effect can be caused by water adsorption in micropores, as according to the theory of volume filling of pores [58], the free energy of water in micropores does not practically depend on its localization there. Adsorbed water can be frozen if its free energy becomes equal to that of ice at a given temperature. If such a temperature has not been reached, freezing of water does not occur, and the unfrozen water concentration remains

practically unchanged. The portion of the graph of ΔG as a function of C_{uw} to the left of the vertical line (Figure 12) corresponds to freezing of water in micropores; and that to the right is associated with water in larger pores or weakly bound water on the outer surface of the adsorbent particles. The points at the abscissa corresponding to the vertical lines determine the concentration of water adsorbed in micropores (Table 6, C_{uw}^{mp}).
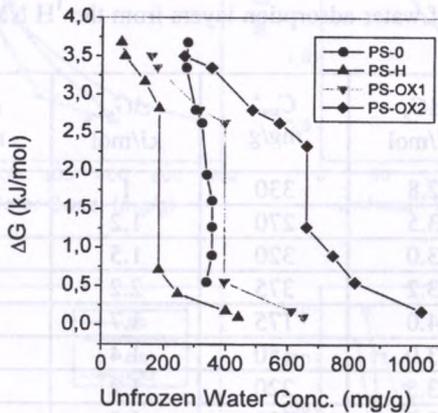
Fig. 12. Changes in the Gibbs free energy of the interfacial water in the aqueous suspensions of activated carbons

Tab. 6. Characteristics of the interfacial water layers in the frozen aqueous suspensions of carbons

Adsorbent	ΔG_{max} kJ/mol	C_{uw}^{max} mg/g	C_{uw}^{mp} mg/g	γ_S mJ/m^2	S_{BET} m^2/g
PS-0	4.2	810	380	58	1174
PS-H	4	500	190	33	1184
PS-OX1	4	700	400	63	1162
PS-OX2	4	1200	650	112	1201

As is seen from the data in Table 6, the free surface energy (γ_S) and content of unfrozen water (C_{uw}^{max}) decrease for PS-H. It is in agreement with the notion that such a treatment results in a decrease in the surface concentration of oxidized groups, which can form hydrogen-bonded clusters of water molecules. Additionally, for PS-H, a sharp decrease in the concentration of water adsorbed in micropores is seen. This effect can be explained by lowering of the accessibility of micropores for water molecules due to increase in the

hydrophobic properties of the adsorbent surfaces reduced by H_2. When the carbon surfaces are treated with hydrogen peroxide (PS-OX1, PS-OX2), an increase in the bound water concentration is observed in comparison with PS-0 due to formation of additional polar groups, which can form hydrogen-bonded complexes with water molecules in micropores and on the outer surface of adsorbent particles.

6.2. Water adsorbed on zeolites. Zeolite samples [62,63] were synthesized according to the technique described elsewhere [64] on the basis of fumed alumina-silicas. Such a procedure allowed us to simplify the synthesis of zeolites while alumina-silica served as a source for formation of the both oxides in the zeolite crystal lattice.

The zeolites were synthesized using alumina-silica with molar ratios SiO_2/Al_2O_3 equal to 131, 100, 26 and 19.5 for preparation of samples 1-4 (Table 7), respectively. The template was tetrapropylammonium bromide. In order to prepare a reaction mixture, sodium hydroxide and template were dissolved in distilled water; then a suitable amount of alumina-silica was added to this solution mixed. In terms of oxides the component ratios in the reaction mixture were as follows: $Na_2/SiO_2 = 0.05$, $[(C_3H_7)_4N]_2O/SiO_2 = 0.04$, $H_2O/Na_2O = 300$.

Tab. 7. Structural characteristics of zeolites

Sample	C_{Al2O3} wt%	S_{BET} m^2/g	V_p cm^3/g
1	1.96	515	0.26
2	3.15	482	0.23
3	7.38	475	0.26
4	8.95	450	–

A X-ray diffraction study was made with a DRON-UMI (LOMO) diffractometer using Ni-filtered Cu Kα radiation. The comparison of the XRD patterns of the prepared samples with the literature data on ZSM-5 [65] shows that these samples correspond to ZSM-5, whose degrees of crystallinity were 94-96 %. The specific surface area S was measured by the method of thermal desorption of argon; the pore volume V_p was determined using methanol adsorption isotherms. The values obtained are listed in Table 7.

As follows from the data listed in Table 8, the concentration of water adsorbed in zeolite pores and the free surface energy of adsorbents (with the exception of the sample containing 3.15 wt. % of Al_2O_3) decrease with the aluminum content. At the same time, the maximum decrease in the free energy

in a layer of bound water is practically the same for all the studied zeolites and about twice as large as the corresponding value for silicalite. Under these conditions, the total adsorbent pore volume is filled by water only for a sample at $C_{Al2O3} = 1.96$ wt.%. The observed regularity disagrees with the data presented in [66] for adsorption of water vapors in zeolites differing in the concentration of Al in their crystal lattice. The cause of the observed features may be two main factors, namely change in the structure of water polyassociates with increasing concentration of Al and variation of conditions for the competing sorption of water and gases in air. Really, in the situation of a high degree of hydration of the surfaces, water not only interacts directly with primary adsorption sites but also forms large clusters near Brönsted acid sites [67]. However, the high acidity is characteristic only of a relatively small portion of surface hydroxyl groups, which is evidenced for by the data of calorimetric titration [68]. With increasing concentration of aluminum, the content of such active OH groups decreases, and, as a consequence, one may also observe a decrease in the sizes of clusters of water molecules adsorbed on the surface. Thus, despite the increase in the concentration of primary sites for water adsorption, the enhancement of the concentration of aluminum can be accompanied with a reduction of the degree of hydration of the zeolite surfaces.

Tab. 8. Characteristics of interfacial water layers in aqueous suspensions of zeolites

C_{Al2O3} wt%	C^{max} mg/g	ΔG_{max} kJ/mol			γ_S mJ/m^2
		Water	Air	CDCl$_3$	
0*	55	3.2	-	-	5
1.96	250	6.1	4.8	3.0	37
3.15	80	6.1	5.5	2.3	6
7.38	120	6.0	-	6.0	26
8.95	85	6.2	5.0	4.0	19

If adsorption of water is affected in air, there may appear a second factor that affects the dependence of the degree of hydration of the surface on the aluminum content in a sample. Owing to the presence of air, the zeolite surface can adsorb simultaneously not only water but also molecules of nitrogen and oxygen that are not able to form hydrogen-bonded complexes with surface hydroxyl groups and are adsorbed predominantly on more hydrophobic portions of the surface. With increasing sizes of clusters of water adsorbed on the surface, some portion of the adsorbed gases must be removed from the surface. Then the value of adsorption of water should depend on the relationship

between the free energy of formation of water clusters and that of desorption of gas molecules from the surface. In this situation, the formation of water clusters on hydrophilic sites of the surface may be energetically less favourable than adsorption of gas molecules on hydrophobic portions of this surface. As the content of aluminum in the zeolite increases, the number of primary sites for adsorption of water increases too, but the water clusters formed nearby these sites make contact predominantly with hydrophobic portions of the surface created by siloxane bridges. As a result, one can observe an effect that manifests itself in a decrease in the free surface energy of zeolites with increasing content of aluminum in their lattice.

7. CONCLUSIONS

The free surface energy of unmodified and modified oxides in the aqueous medium may vary in the range of 100-1100 mJ/m^2 depending on the nature of the adsorbents, and the thickness of the interfacial water disturbed by the surfaces ranges from 3 to 45 statistical monolayers. This is connected with the fact that in aqueous medium a high contribution of polarization and structural components to measured values of surface energy is observed. The magnitude of these components depends not only on the morphology and chemical structure of adsorbent surfaces but also on the structure of inter-particle aggregates as well as on concentration of a solid phase in the aqueous suspension. For this reason for the same material, the thickness of the layer of adsorbed water may vary depending on conditions of preparation of the adsorbent in a wide range. The increase in the thickness of layer of surface-structurized water leads to a decrease in the adsorption ability of the adsorbent.

Maximum values of the free surface energy are observed for samples characterized by the heterogeneous surfaces (carbosil having a small amount of pyrocarbon deposits, the mixture of silica with methylsilica, amorphous silica previously wetted). Specially separated fragments of the surfaces of the above adsorbents are characterized by different values of dissociation constants of the surface hydroxyl groups and by different affinities to protons. At the same time a polarization of the adsorbent surface takes place. It can be assumed that the thickness of the layer of adsorbed water is strongly affected by the surface charge distribution nonuniformity connected with appearance of oppositely charged fragments, and the field created by these fragments influences the orientation of dipoles of water molecules. The appearance of surface charges is also possible in the zones of interparticle contacts. For this reason in the case of low dispersion materials, the values of the free surface energy and layer thickness of adsorbed water in the aqueous suspensions are not determined by

hydrophilic-hydrophobic properties of these materials but by capability of the surface to polarization.

The maximum layer thickness for water adsorbed in porous adsorbents cannot substantially exceed their pore radius. Therefore, when the action radius for surface forces is smaller than the pore radius, the layer thickness for water adsorbed on the surface is governed mainly by the surface concentration of hydrophilic sites. If the surface potentials of the opposite walls of a pore are overlapped, all the water filling the pore is bound to the surfaces. The freezing temperature for water in such a pore is governed by the pore sizes and force of interaction between the surface and water. The free surface energy value measured for such adsorbents determines the intensity of interactions between water molecules and pore surface. In the case of chemically modified carbonaceous adsorbents the comparison between values of their free surface energies in an aqueous medium makes it possible to obtain valuable information on the constitution of their surface.

REFERENCES

[1] Su M.Y., Nalcioglu O., *J. Colloid Interface Sci.*, 160, 332 (1993).
[2] Vashman A.A., Pronin I.S., *Nuclear Magnetic Relaxation Spectroscopy*, Energoatomizdat, Moscow, 1986.
[3] Bradl S., Lang E.W., Turner J.Z., Soper A.K., *J. Phys. Chem.*, 98, 8161 (1994).
[4] Bourdin V., Germanus A., Grenier P., Karger J., *Adsorption*, 2, 205 (1996).
[5] Rolle-Kampczyk U., Karger J., Caro J., Noack M., Klubes P., Rohl-Kuhn B., *J. Colloid Interface Sci.*, 159, 366 (1993).
[6] Delville A., Letellier M., *Langmuir*, 11, 1361 (1995).
[7] Derjaguin B.V., Churaev N.V., Muller V.M., *Surface Forces*, Consultants Bureau, New York, 1987.
[8] Lucham P.F., de L. Costello B.A., *Adv. Colloid Interface Sci.*, 44, 183 (1993).
[9] Rudzinski W., Charmas R., *Adsorption*, 2, 245 (1996).
[10] Meagher L., Pashley R.M., *J. Colloid Interface Sci.*, 185, 291 (1997).
[11] Zilberbrand M., *J. Colloid Interface Sci.*, 192, 471 (1997).
[12] Dukhin S.S., *Adv. Colloid Interface Sci.*, 44, 1 (1993).
[13] Van Oss C.J. *Interfacial Forces in Aqueous Media*, Marcel Dekker, New York, 1994.
[14] Woodward J.T., Gwin H., Schwarts D.K., *Langmuir*, 16, 2957 (2000).
[15] Drummond C.J., Chan Y.C., *Langmuir*, 13, 3890 (1997).

[16] Van Giessen A.E., Bukman D.J., Widom B., *J. Colloid Interface Sci.*, 192, 257 (1997).

[17] Duncan D., Li D., Gayados J., Newmann A.W., *J. Colloid Interface Sci.*, 169, 256 (1995).

[18] Voelkel A., *Critical Rev. Analitical Chem.*, 22, 411 (1991).

[19] Park S.-J. Brendle M., *J. Colloid Interface Sci.*, 188, 336 (1997).

[20] Bogillo V.V., Turov V.V., Voelkel A., *J. Adhesion Sci. Technol.*, 11, 1513 (1997).

[21] Hillig W.B., *J. Crystal Growth.*, 183, 463 (1998).

[22] Tabony J., *Progr. NMR Spectr.*, 14, 1 (1980).

[23] Gorbunov B.Z., Lazareva L.S., *Kolloid. Zh.*, 51, 1062 (1989).

[24] Bogdan A., Kulmala M., Gorbunov B., Kruppa A., *J. Colloid Interface Sci.*, 177, 79 (1996).

[25] Bartell L.S., *J. Phys. Chem.*, 99, 1080 (1995).

[26] Yazykina I.V., Kvilidze V.I., Krasnushkina A.V., *Kolloid. Zh.*, 49, 1188 (1987).

[27] Kvilidze V.I., Adonkin A.A., Krasnushkina A.V., Kurzaev A.B., *Bound Water in Dispersion Systems*, N 3, MSU, Moscow, 1974.

[28] Kashchiev D., Van Rosmalen G.M., *J. Colloid Interface Sci.*, 169, 214 (1995).

[29] Rabinovich Ya., Derjaguin B.V., Yudovich M.E., Kochetkova E.I., Sokolova I.P., *Dokl. AN USSR*, 311, 905 (1990).

[30] Derjaguin B.V., Ovcharenko F.D., Churaev N.V. (Eds.), *Water in Dispersion Systems*, Khimia, Moscow, 1989.

[31] Hansen E.W., Stocker, M., Schmidt, R., *J. Phys. Chem.*, 100, 2195 (1996).

[32] Gun'ko V.M., Zarko V.I., Turov V.V, Voronin E.V., Tischenko V.A., Chuiko A.A., *Langmuir*, 11, 2115 (1995).

[33] Turov V. V., Bogillo V. I., Leboda R., *Extended Abstracts of EUROFILLERS' 95*, Sept. 11-14, 1995, Mulhouse, France, p. 131.

[34] Turov V.V., Leboda R., Bogillo V.I., Skubiszewska-Zięba J., *Proceedings of Second International Symposium "Effects of Surface Heterogeneity in Adsorption and Catalysis on Solids*, Poland-Slovakia, September 4-10, 1995, p. 99.

[35] Turov V.V., Zarko V.I., Chuiko A.A., *Ukr. Khim. Zh.*, 69, 1262 (1995).

[36] Glushko V. P. (Ed.), *Handbook of Thermodynamic Properties of Individual Substances,* Nauka, Moscow, 1978.

[37] Abragam, A., *The Principles of Nuclear Magnetism*, Oxford University Press, Oxford, 1961.

[38] Frolov Yu. G. *Surface Phenomena and Dispersion Systems*, Khimia, Moscow, 1982.

[39] Churaev N.V., *Kolloid. Zh.*, 54, 169 (1992).
[40] Attard P., Ursenbach C.P., Patay G.N., *Phys. Rev.*, 45, 7621 (1992).
[41] Attard P., Parker J.L., *J. Phys. Chem.*, 96, 5086 (1992).
[42] Luchom P.F., Costello B.A.D., *Adv. Colloid Interface Sci.*, 44, 183 (1993).
[43] Claesson P.M., Blomberg E., Froberg J.C., Nylander T., Arnebrant T., *Adv. Colloid Interface Sci.*, 57, 161 (1995).
[44] Turov, V.V.; Barvinchrnko, V.N., *Colloids Surf. B*, 8, 125 (1997).
[45] Turov V.V., Leboda R., *Adv. Colloid Interface Sci.*, 79, 173 (1999).
[46] Turov V.V., Bogillo V.I., Chuiko A.A., *Ukr. Khim. Zh.*, 59, 580 (1993).
[47] Turov V.V., Chuiko A.A., Skiba V.V., *Ukr. Khim. Zh.*, 59, 804 (1993).
[48] Turov V.V., Chuiko A.A., Skiba V.V., *Ukr. Khim. Zh.*, 60, 156 (1994).
[49] Claesson P.M., Christenson H.K., Ber J.M., Neuman R.D., *J. Colloid Interface Sci.*, 172, 415 (1995).
[50] Spalla O., Kekichiff P., *J. Colloid Interface Sci.*, 192, 43 (1997).
[51] Atkins D., Kekichiff P., Spalla O., *J. Colloid Interface Sci.*, 188, 234 (1997).
[52] Turov V.V., Mironiuk I.F., *Colloids Surf. A*, 134, 257 (1998).
[53] Gun'ko V.M., Turov V.V., Zarko V.I., Voronin E.F., Tischenko V.A., Dudnik V.V., Pakhlov E.M., Chuiko A.A., *Langmuir* 13, 1529 (1997).
[54] Turov V.V., Leboda R., Bogillo V.I., Skubiszewska-Zięba J., *J. Chem. Soc., Faraday Trans.*, 93, 4047 (1997).
[55] Gun'ko V.M., Zarko V.I., Turov V.V., Leboda R., Chibowski E., Holysz L., Pakhlov E.M., Voronin E.F., Dudnik V.V., Gornikov Yu.I., *J. Colloid. Intrface Sci.*, 198, 141 (1998).
[56] Gun'ko V.M., Zarko V.I., Turov V.V., Leboda R., Chibowski E., Pakhlov E.M., Goncharuk E.V., Marciniak M., Voronin E.F., Chuiko A.A., *J. Colloid Interface Sci.*, 220, 302 (1999).
[57] Gun'ko V.M., Leboda R., Skubiszewska-Zięba J., Turov V.V., Kowalczyk, P., *Langmuir*, 17, 3148 (2001).
[58] Dubinin, M.M., in: *Progress in Surface and Membrane Science*, Cadenhead, D.A. (Ed.), Vol. 9, Academic Press, New York, 1975, p. 1.
[59] Legrand A.P. (Ed.), *The Surface Properties of Silicas*, Wiley, New York, 1998.
[60] Leboda R., Turov V.V., Charmas B., Skubiszewska-Zięba J., Gun'ko V.M., *J. Colloid Interface Sci.*, 223, 112 (2000).
[61] Leboda R., Turov V.V., Tomaszewski W., Gun'ko V.M., Skubiszewska-Zięba J., *Carbon,* galley proof.

[62] Turov V.V., Brei V.V., Khomenko K.N., Leboda R., *Microprous and Mesoporous Materials* 23, 189 (1998).
[63] Turov V.V., Brei V.V., Khomenko K.N., Leboda R., *Adsorption Sci. Technol.*, 18, 75 (2000).
[64] Grose, R.W., Flanigen, E.M., *US Patent* 4 061 724 (1977).
[65] Argauer, R.J., Landolt, G.R., *US Patent* 3 702 886 (1972).
[66] Tsutsumi K., Mizoe K. *Proseeding of International Symposium on Adsorption*, June 13-25, Kyoto, Japan, 1988, p. 75.
[67] Buzzoni R., Bordiga S., Ricchiardi G., Lambert C., Zecchina A., *Langmuir*, 12, 930 (1996).
[68] Drago R.S., Dias S.C., Tottealba M., de-Lima L., *J. Am. Chem. Soc.*, 119, 4444 (1977).

CURRICULA VITAE

Vladimir Turov was born in Ukraine in 1951. Graduated from Department of Radiophysics of Kiev State University (1973). In the 1985 received Ph.D. degree in Pisarzhevski Institute of Physical Chemistry (Kiev).

Professional experience: 1975 – Engineer in Institute of Semiconductors (Kiev); 1975-1980 – Senior Engineer in Institute of Physical Chemistry; 1980-1987 – Leading Engineer in Inst. Phys.Chem., 1987-1989 – Researcher in Institute of Surface Chemistry; 1989-2000 – – Senior Researcher in Institute of Surface Chemistry.

Specialization: Physical Chemistry, Surface Chemistry, NMR.
Current research interest: NMR spectroscopy of mobile phases.
Number of papers in refereed journals: 90.
Number of communications to scientific meetings: 30.

Vladimir Gun'ko was born in Ukraine in 1951. He received his M.Sc. in Theoretical Physics from Dniepropetrovsk State University. In 1983, Gun'ko received his Ph.D. degree in chemical sciences from Institute of Physicoorganic Chemistry and Coil Chemistry (Kiev) and Sc.D. (1995) from the Institute of Surface Chemistry, National Academy of Sciences of Ukraine in Kiev.

Professional experience: 1973-1976 – Engineer in Dniepropetrovsk State University; 1976-1978 – Senior Engineer in Institute of Physo-Organic Chemistry and Coil Chemistry (Kiev); 1978-1985 – Junior Researcher in Int. of Phys-Org. Chem. and Coil Chem.; Senior Researcher in Institute of Surface Chemistry, NASU (Kiev);
1991-1996 – Head of Laboratory in Institute of Surface Chemistry NASU; 1996-2000 – – Leading Resercher in Institute.
Specialization: theoretical chemistry, quantum chemistry, programming, physical chemistry (kinetics, colloidal chemistry, physical of solid state).
Current research interest: adsorption, enviromental chemistry.
Number of papers in refereed journals: about 150.
Number of communications to scientific meetings: 50.

Roman Leboda was born in Poland in 1943. Graduated from Maria Curie-Skłodowska University in Lublin (1967). Hi obtained the Ph.D. and Sc.D. degrees he obtained in 1974 and 1981, respectively. He received the professor title in 1989. Specialization: Physical Chemistry, Chromatography, Physical-Chemistry of Surface, Adsorption.
Current research interest: preparation of carbon and carbon-mineral adsorbents – surface properties, its modification and application, analysis of trace substances in air, water and soil by chromatographic methods; sample preparation.
Member of Polish Chemical Society and International Adsorption Society. Visiting Professor in Institute fur Anorganische and Analytische Chemie, J. Gutenberg Universität, Mainz (1982-83). President of the Lublin Division of the Polish Chemical Society (1989-93).
He organized the six Polish-Ukrainian Symposia: *Theoretical and Experimental Studies of Interfacial Phenomena and Their Technological Applications.*
Number of papers in refereed journals: about 250 and 30 patents.
Number of communications to scientific meetings: about 150.
Number of books: 2.

Volodimyr Brei was born in Ukraine in 1953. Graduated from Moscow State University (1976); post-graduate student of the Pisarzhevski Institute of Physical Chemistry (Kiev, 1979-81); doctor of chemical sciences (1982).

Professional experience: 1976-1986 – engineer, post-graduate student, senior researcher of the Pisarzhevski Institute of Physical Chemistry; 1986-1991 – Head of laboratory; 1991 – Deputy--director of the Institute of Surface Chemistry of the National Academy of Sciences, Kiev.

Specialization: surface chemistry of oxides, catalysis, adsorption.

Present key interest: synthesis and study of super-acid solids and mesoporous oxides, chemical modification of the surfaces of dispersed oxides.

Publications: 65 articles in chemical scientific journals, 9 patents.

E mail: brei@alfacom.net ; tel. (38044)4448230